Received: 16 February 2022 | Revised: 28 May 2022 | Accepted: 16 June 2022

DOI: 10.1111/ffe.13776

SPECIAL ISSUE ARTICLE

FFEMS Fatigue & Fracture of Engineering Materials & Structures WILEY

Modeling of fatigue failure mode in U-rib to deck joints in orthotropic bridge structures

Haibo Yang[1,2] | **Ping Wang**[2] | **Hongliang Qian**[2] | **Pingsha Dong**[3]

[1]College of Water Conservancy and Civil Engineering, Shandong Agricultural University, Taian, China

[2]School of Ocean Engineering, Harbin Institute of Technology at Weihai, Weihai, China

[3]Department of Naval Architecture and Marine Engineering, University of Michigan, Ann Arbor, Michigan, USA

Correspondence
Ping Wang, School of Ocean Engineering, Harbin Institute of Technology at Weihai, Weihai 264200, China.
Email: nancywang@hit.edu.cn

Funding information
National Key R & D Program of China, Grant/Award Number: 2019YFB1600702; Natural Science Foundation of China, Grant/Award Numbers: 51605116, 51678191

Abstract

Various fatigue failure modes (i.e., cracking position and orientation with respect to a weld) can develop in welded rib to deck connections in orthotropic bridge deck structures. After demonstrating its effectiveness in correlating fatigue test data covering different failure modes, the master S-N curve method was then adopted in this study for determining the critical failure mode in welded U-rib to deck connections. These include considerations of additional failure modes potentially present in double-sided welds between U-rib and deck versus the traditional single-sided weld design. The effects of weld penetrations and test loading conditions on failure mode development have been quantitatively established by means of the master S-N curve method.

KEYWORDS

bridge engineering, double-sided weld, fatigue failure mode, master S-N curve, orthotropic bridge deck, traction structural stress

1 | INTRODUCTION

Long-span steel bridges are popularly constructed using orthotropic bridge deck (OBD) structures, such as in the Hong Kong–Zhuhai–Macau bridge.[1,2] OBDs consist of longitudinal and transverse ribs and crossbeams, providing the advantages of lightweight construction and significant load-bearing capability.[3–5] Fatigue failure cracks have been observed in deck-rib-crossbeam connections.[6] The complex connection types of the bridge deck, U-rib, and web crossbeam lead to the serious problem of fatigue failure crackings and large potential safety hazards on bridge engineering. The safety of the long-span steel bridges in service is significantly affected, and the service life of steel bridges is shortened by the fatigue failure crackings. It's urgent to study the fatigue failure mode and life prediction of the OBD.

Researchers have studied over 7000 fatigue crackings on steel bridge decks and obtained the distribution and propagation orientation of fatigue crack defects,[7] as shown in Figure 1. The results show that the proportions of fatigue cracks in the deck-crossbeam joints, U-rib to deck welds, U-rib to crossbeam joints, and butt joints of U-rib are 3.0%, 50.0%, 40.0%, and 7.0%, respectively.[8] In addition, fatigue cracks originated at the weld toe or root of the bridge deck and propagated along the thickness orientation. Fatigue cracks initiated at the weld toe of U-ribs and went along the U-rib thickness orientation.[9] Besides, some fatigue cracks were observed in the weld throat and web crossbeams, which propagated through the weld throat, and the crossbeam plane.

The crack propagation modes and orientations are affected by the bridge design details.[10–12] Researchers have conducted theoretical studies and fatigue tests on U-rib-to-deck connections, including single-sided weld joints,[13–15] butt weld joints,[16,17] and double-sided weld joints.[18]

The local stress concept, including the notch structural stress method with various fictitious notch radii, is

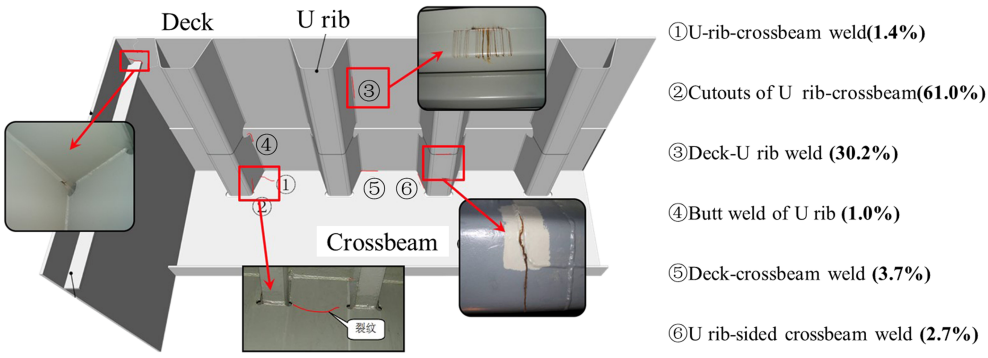

FIGURE 1 Summary of fatigue failure modes in orthotropic bridge deck (OBD)[7] [Colour figure can be viewed at wileyonlinelibrary.com]

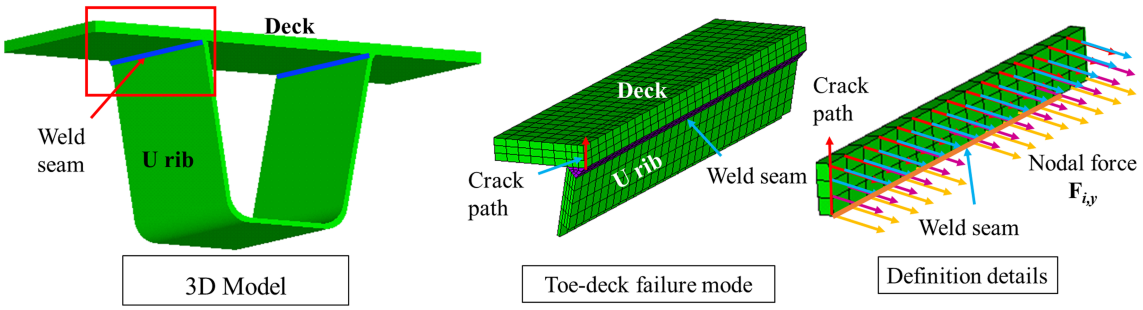

FIGURE 2 Nodal forces and moments along the weld seam[47] [Colour figure can be viewed at wileyonlinelibrary.com]

investigated and considered by Karakas et al.[19–22] Besides, the notch stress method has been extended for evaluating fatigue performances of welded structures in multiaxial stress states by Tao,[23] Luca,[24] and Ran.[25] The recommended evaluation methods on the fatigue properties of OBD are associated with some limitations.[15,26–29] Pei and Dong [30] further extended this method to a low-cycle fatigue regime and came up with a structural strain method, which can correlate both high- and low-cycle fatigue data weldments made from different base metals into a master E-N curve. Such problems can be tackled using the unified master *S-N* curve method,[31–36] which is based on the traction structural stress theory[37–39] and used in the pressure vessel and marine welded structures.

In terms of newly developed welded joint types with advanced techniques, some researchers recently proposed a method with innovative welded joints in OBD, that is, double-sided U-rib to deck welds, employed in the Wuhan Yangtze River Bridge.[18] Other failure cracks are seldom investigated, that is, extending along the weld throat and U-rib thickness. According to Eurocode 3, the weld penetration of the deck and transverse U-rib should not be less than 75%, while the location and constraint of fatigue load have not been specified.[40] The constraint forms and load positions used in existing fatigue tests differ significantly,[41,42] and the effect on the fatigue properties is still under investigation. Researchers have proposed that double-sided weld joints can improve the overall stiffness of U-rib-to-deck joints.[43,44]

In this paper, the fatigue failure modes of double-sided weld joints are investigated using the master *S-N* curve method and the test results in previous works.[26,41,42,45–48] The master *S-N* curve method is applied to evaluate the fatigue properties and fatigue failure modes of double-sided weld joints. In addition, the disadvantages of double-sided weld joints are discussed in light of the inspection detection probability. The effect of double-sided weld joints, loading modes, and weld penetration on fatigue properties is investigated to analyze the fatigue failure mode.

2 | METHODS AND VERIFICATIONS

2.1 | Structural stress-based master *S-N* curve method

The actual stress state of a double-sided weld joint between the bridge deck and the U-rib in an OBD structure can be implemented using the mechanical method. The traction structural stress has been proposed by Dong[49–51] based on the fracture theory and the fatigue propagation law.

After the weld seam and elements of the weld toe or root are determined, nodal forces and moments of nodes along a specific weld seam can be extracted from numerical simulation analysis results (Figure 2). In this case, the toe-deck failure mode is detailed illustrated, and fatigue crack originates at the deck weld toe and propagates along the deck thickness orientation. The internal stress of the plane along the thickness orientation consists of the normal stress $\sigma_x(y)$ and the in-plane shear stress $\tau_{xy}(y)$. The normal stress $\sigma_x(y)$ consists of the membrane stress σ_m, and the bending stress σ_b, which can be calculated by Equations (1)–(3).

$$\sigma_m = \frac{1}{t}\sum_{i=1}^{n} F_{i,y} \tag{1}$$

$$\sigma_b = \frac{6}{t^2}\sum_{i=1}^{n} F_{i,y} \times \left(y_i - \frac{t}{2}\right) \tag{2}$$

$$\sigma_s = \sigma_m + \sigma_b \tag{3}$$

where $F_{i,y}$ is the nodal force of the nodes along the weld seam, t is the thickness of the base metal, and y_i represents the nodal coordination.

The stress amplitude at potential planes can be obtained using Equations (1)–(3). As is known, welded structures with various thicknesses under different fatigue loads or combinations. Therefore, effects of depth and load mode can be calculated and described in equivalent structural stress (ESS), in consideration of equated depth and bending load ratio.

First, a bending load ratio, namely, bending stress to structural stress, can be calculated by Equation (4). Then, the load mode parameter I(r) can be calculated using Equation (5), which was obtained based on numerical and analytical methods by Dong. Meanwhile, the effect of base metal depth on structural stress is corrected with the equation $t^{*(2-m)/2m}$. In summary, the ESS ΔS_s was obtained in consideration of the equated thickness t^*, bending ratio r, the parameter of loading mode I(r), and traction structural stress range $\Delta\sigma_s$ by Equation (6). The ESS range ΔS_s versus the fatigue cyclic life N, that is, a correlation in the master S-N curve, can be obtained using master S-N curve parameters C_d and h (plotted in Table 1), and $m = 3.6$ using Equation (7).[49–51]

$$r = \sigma_b/\sigma_s \tag{4}$$

$$I(r)^{1/m} = 0.0011r^6 + 0.0767r^5 - 0.0988r^4 + 0.0946r^3 + 0.0221r^2 + 0.014r + 1.2223 \tag{5}$$

$$\Delta S_s = \frac{\Delta\sigma_s}{t^{*(2-m)/2m} \cdot I(r)^{1/m}} \tag{6}$$

$$N = (\Delta S_s/C_d)^{1/h} \tag{7}$$

2.2 | Fatigue test conditions and numerical simulation

Three-point bending fatigue experiments were performed by You in HZU.[48] The fabrication[52] and weld technology were determined according to the Wuhan Yangtze River Bridge and Eurocode 3.[40] Figure 3A,B illustrates the experimental configuration and specimen dimensions.[48] In actual bridges, random traffic loadings are secondary load types. The stress state of bridge deck plates is the secondary bending stress based on the continuum structural mechanics. It has been verified that the orientation of the longitudinal U-rib is the weak orientation of OBD. Therefore, fatigue performances of OBD can be investigated by three-point bending fatigue tests, and in this case, fatigue test specimens were supported using bolt connections. Consistent-amplitude proportional fatigue load was applied to the top central location of the deck plate using a rubber lining.

To validate test results, fatigue specimens of single and double U-ribs with various weld penetrations and weld leg sizes were tested. In the experiments, the groove angle was 55° and the material of the specimens was S355 (EN, $\sigma_y = 355$ MPa). The traction structural stress was calculated according to the calculation procedure described in Section 2.1, and the fatigue properties were determined using the employed method.

Representative finite element models (FEMs) of specimens were developed to replicate the experimental tests (Figure 3C). The constraints and load setup were consistent with the tests. The FEMs were supported at both ends of the deck, and a load was applied to the

TABLE 1 Master S-N curve parameters[49]

Statistics base	Mean curve	$+2\sigma$	-2σ	$+3\sigma$	-3σ
C_d	19930.2	28626.5	13875.7	34308.1	11577.9
h	−0.3195	−0.3195	−0.3195	−0.3195	−0.3195

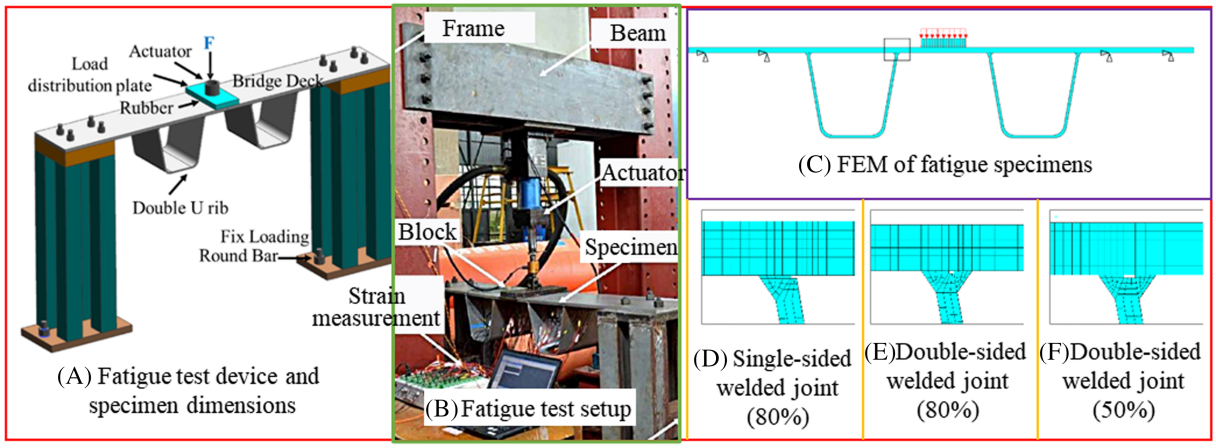

FIGURE 3 (A–F) Fatigue test device and finite element model (A and B were in previous works[47,48]) [Colour figure can be viewed at wileyonlinelibrary.com]

distribution plate. The Solid185 element type in ANSYS software was used, that is, hexahedral solid elements with bilinear kinematic hardening. Single-sided and double-sided U-rib to deck welds were developed in OBD (Figure 3D–F).

2.3 | Validation of the master S-N curve method

The experimental and numerical results can be compared to validate the accurate evaluation of the employed method. The local stress distribution, initiation location, and propagation orientation of the fatigue cracks were obtained from fatigue tests of eight specimens using an electron microscope.

Taking measured stress amplitudes of the specimen SS80 as an example, a comparison between the measured stress range[48] and numerical ESS range is illustrated in Figure 4. The actual stress range of critical positions at U-rib components was measured with strain gauges at positions U1-4 and U1-6. Meanwhile, the ESS of these positions can be obtained using the method in this paper. It should be noted that the ESS is a constant value and can be calculated based on initiation and propagation procedures but not include the fracture stage. It can be seen from comparative results that the ESS is averagely higher by 7.14% than measured stress. A specific distance away from the weld toe of U-rib to deck welds is responsible for lower stress of measured stress results.

Fatigue cracks in specimens without fracture fail were tested using magnetic particle testing technology and a high-power electron microscope. It can be concluded from comparative results (Figure 5) that the fatigue crack of the specimen SD80 initiated at the deck weld toe and

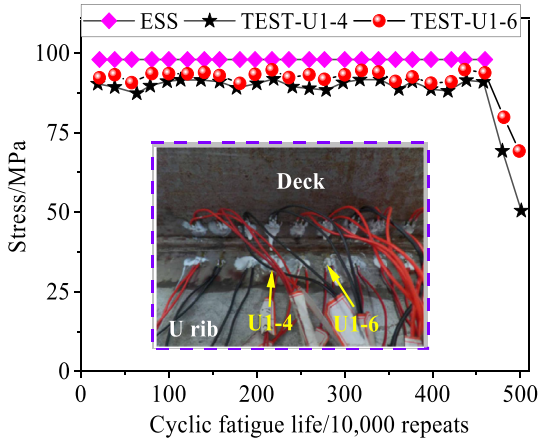

FIGURE 4 Comparison of measured stress[48] and equivalent structures stress (ESS) [Colour figure can be viewed at wileyonlinelibrary.com]

extended along the deck thickness. The specimen SS80 cracking occurred first at the U-rib weld toe and propagated along the U-rib thickness orientation. Fatigue crackings of the specimen DD80 and DS80 initiated at the external and internal weld toes and grew along the deck thickness, respectively.

In both experimental and numerical results, fatigue cracks of each specimen originated from the same position and propagated in the same orientation. Besides, an advanced technology, the ultrasonic imaging phased-array technique, has been beginning to be employed to research crack defects and measure crack depth and length.[53]

The cyclic life of crack propagation was determined by the point where the nominal stress decreased suddenly in the σ_n-N curves.[54] The stress extrapolation method was used according to Eurocode 3,[40] and the hot-

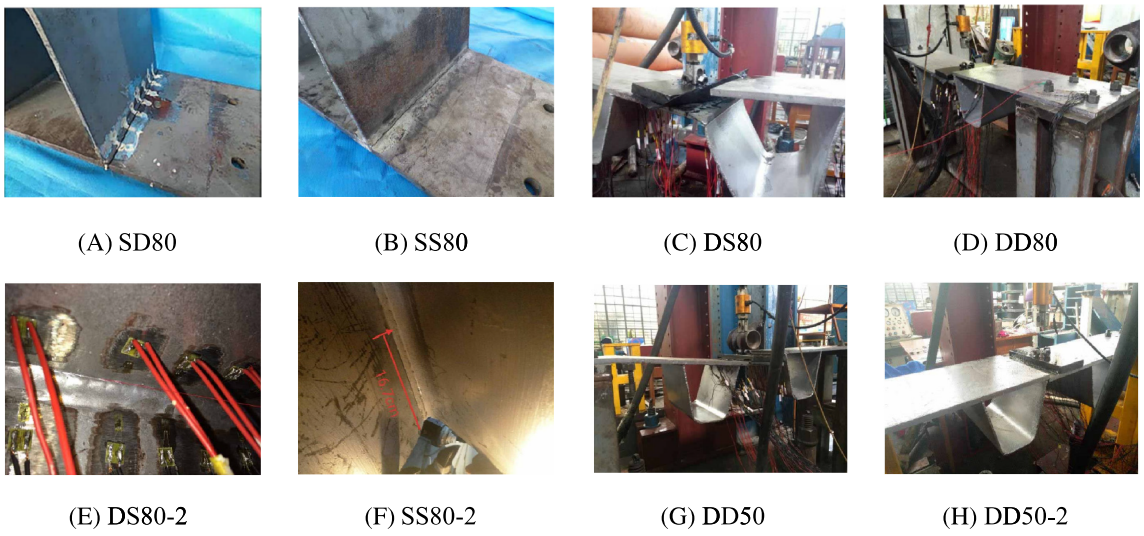

FIGURE 5 (A–H) Fatigue test results and failure modes[48] [Colour figure can be viewed at wileyonlinelibrary.com]

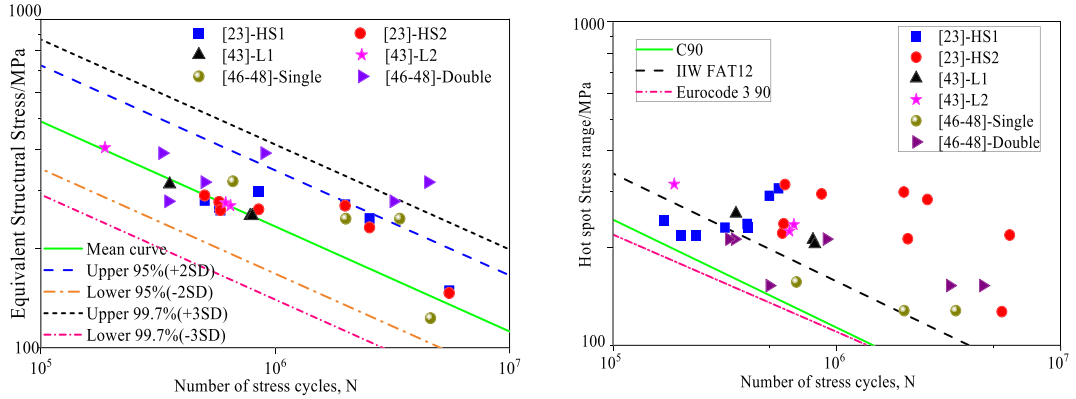

(A) Master S-N curve method (B) Recommended methods

FIGURE 6 (A,B) The correlation between various methods and fatigue test results[26,42,45–47] [Colour figure can be viewed at wileyonlinelibrary.com]

spot stress was determined. The traction structural stresses of the weld root and toe were obtained using the employed method.

In addition, the fatigue tests in references by Aygul[26] and Cheng[42] at SJTU were investigated. The fatigue test data were analyzed, and the test conditions were introduced by team members Wang[31] and Yang.[45–47] Fatigue test specimens of OBD consisted of open I-shaped and closed U-shaped rib components. It is worth noting that tensile fatigue tests of U-rib to deck welds were conducted to establish S-N curves for predicting welded joints in OBD. However, three-point bending fatigue tests of OBD components were carried out and analyzed using the master S-N curve method in this paper. Especially, two-span fatigue specimens with single- and double-sided weld joints were analyzed, and a systematic parameterized analysis was implemented for extension into practical design guidance or specifications.

The aim of citing experimental data from various references is to validate the applicability and accuracy of the employed method for analyzing fatigue properties of OBD components. The ESS is presented in the contour of the master S-N curve (Figure 6A). The hot spot stresses of the test specimens were obtained using the extrapolation method with the corresponding *S-N* curves (Figure 6B).

Fatigue testing results of Aygul, Cheng, and You were evaluated with the *S-N* curves of C90, IIW FAT12, and Eurocode3 FAT90. All sets of experimental data fall within the 99% confidence interval of master S-N curves. The fatigue test data are covered in the narrow band. Predicted structural stress was in good agreement with test result data. The standard deviation of ESS results and the master *S-N* curve method was 0.28.

Predicted results using the hot-spot stress method were conservative with corresponding *S-N* curves with a standard deviation of 0.40. The scatter band of test results extracted using the master S-N curve method was smaller than the hot-spot stress method. Therefore, it has been validated that the unified master *S-N* curve method can capture effects of weld types and penetrations on failure modes of welded joints.

3 | COMPARATIVE AND PARAMETERIZED STUDY ON FATIGUE PROPERTIES

3.1 | Introduction of the analysis scheme

In this section, effects of joint type, weld penetration ratio, loading mode, and weld dimensions on fatigue properties of OBD are investigated using the master S-N curve method, which has been validated by fatigue test data.

Based on test conditions, OBD with two U-ribs in two types of loading modes were analyzed (as plotted in Figure 7A). In loading case I, a fatigue load was applied to the central location with a width of 150 mm. In loading case II, the loading location of loading case I was moved to the left by 75 mm. To guarantee welding quality of U-rib to deck welds and obtain actual weld leg and fused dimensions, the microstructure of U-rib to deck welds was measured using a high magnification optical electron microscope, as plotted in Figure 7B. Besides, the microstructural image of the base material after the welding procedure is indicated in Figure 7B. It can be seen that zone characteristics in heterogeneous welded joints are obvious for identification, including distal and proximal HAZ, fusion line, and fusion zone, which are essentially different from base metal materials. In addition, most of the fusion-welded joints consist of equiaxed crystal, columnar crystal, and dendritic structures, which are absent in base metal materials. Dimensions of double-sided weld joints included the external and internal weld sizes. Figure 7C presents double-sided weld joint dimensions in actual specimens corresponding to actual welded dimensions. In terms of single-sided welded joints, an internal welded seam was absent, and only an external weld seam was designed. The analysis scheme of various factors was determined by considering the double-sided weld joint, loading mode, penetration, and dimensions. Single- and double-sided weld joint dimensions with various weld penetrations are illustrated in Table 2. Hence, four types of welded joints are presented, that is, SW80-W6, DW100-W4, DW75-W4, and DW50-W4.

As demonstrated in many references, fatigue crackings were usually initiated at the welded positions with the stress concentration and sharp change in geometry shape. The initiation position and propagation orientation of fatigue crackings are determined based on the stress concentration distribution. Hypothetical crack initiation positions and propagation orientations in U-rib-to-deck joints are demonstrated in Figure 7D. Hypothetical fatigue failure paths are determined according to observed fatigue cracks in actual bridges. The definition

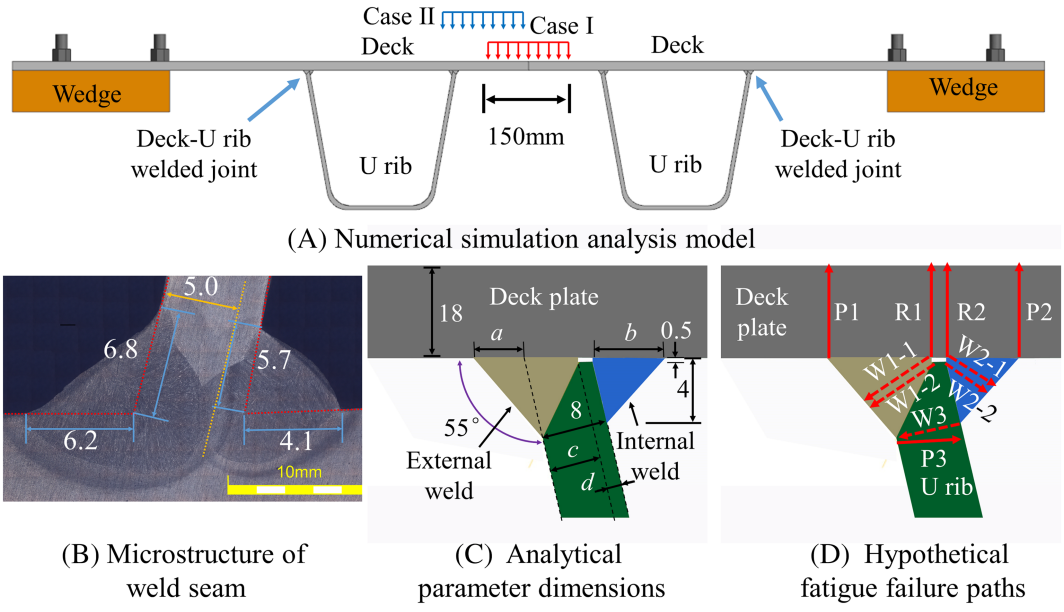

FIGURE 7 (A–D) Constraint conditions, load modes, and failure paths of numerical models [Colour figure can be viewed at wileyonlinelibrary.com]

TABLE 2 Parameterized fatigue analysis SCHEME

Comparative factors	Specimen number	Weld seam type	Weld size/mm		Weld penetration	Fuse/unfused/mm		Load mode
			External weld/*a*	Internal weld/*b*		Fused size/*c*	Unfused size/*d*	
Double-sided weld joint	SW75-W6	Single	6	0	75%	6.4	1.6	Case I
	DW75-W4	Double	4	4	75%	6	2	Case I
	DW75-W6	Double	6	4	75%	6	2	Case I
Load mode and weld penetration	SW80-W6	Single	6	0	80%	6.4	1.6	Case I, II
	DW100-W4	Double	4	4	100%	8	0	Case I, II
	DW75-W4	Double	4	4	75%	6	2	Case I, II
	DW50-W4	Double	4	4	50%	4	4	Case I, II
Weld dimensions	SW80-W6	Single	6	0	80%	6.4	1.6	Case I
	DW80-W4	Double	6	4	80%	6.4	1.6	Case I
	DW80-W6	Double	6	6	80%	6.4	1.6	Case I

TABLE 3 Hypothetical fatigue crack failure paths and corresponding damage modes

Logogram	Initiation location	Propagation orientation	Damage locations
P1	Weld toe of outer weld	Deck thickness	Bridge deck
P2	Weld toe of the inner weld	Deck thickness	Bridge deck
R1	Weld root of outer weld	Deck thickness	Bridge deck
R2	Weld root of the inner weld	Deck thickness	Bridge deck
P3	Weld toe of outer weld of U-rib	U-rib thickness	U-rib
W1-1	Weld root of outer weld near the deck	Outer weld thickness	Outer weld throat
W1-2	Weld root of outer weld near U-rib	Outer weld thickness	Outer weld throat
W2-1	Weld root of inner weld near the deck	Inner weld thickness	Inner weld throat
W2-2	Weld root of inner weld near U-rib	Inner weld thickness	Inner weld throat
W3	Weld toe of outer weld of U-rib	To inner weld toe	U-rib

of various fatigue failure paths in advances aims to cover all possible fatigue crack types and compare traction structural stress amplitudes. The maximum traction structural stress along every weld seam will be analyzed based on the fatigue analysis procedure, respectively. Fatigue crack is more likely to initiate at a location with the maximum structural stress range and high tip stress strength factors and grow along a specific fatigue failure path defined in advance, which can be defined as the main failure mode. In general, the main fatigue crack is likely to originate and propagate with some other micro fatigue cracks.

Meanwhile, Figure 7D presents failure modes of fatigue cracks. The red arrow indicates the propagation path. The start point at one end of the arrow indicates the crack initiation position, while the opposite end points to the crack propagation orientation. Hypothetical fatigue failure paths are summarized in two parts, including failure modes of specimen base metal (P1, P2, P3, R1, and R2) and failure modes of weld seam throat (W1-1, W1-2, W2-1, W2-2, and W3).

Detailed corresponding damage modes are illustrated in Table 3. It should be noted that the fatigue failure mode of welded joints with qualified welding quality can be predicted based on the magnitude of traction structural stress. Poor welding quality and angular misalignments may affect the evaluation accuracy of the employed method in this paper. In cases where traction structural stresses at weld root and weld toe are very close, the fatigue failure modes may be affected by

random factors, such as material and geometric imperfections, in a transition zone region.[55]

3.2 | Fatigue performance of double-sided weld joints

The fatigue properties of double-sided weld joints were analyzed based on loading case I. Different initiation positions and failure modes of the specimens SW75, DW75-4, and DW75-6 were investigated. In Figure 8, the comparative ESS is plotted. The position of the maximum ESS in SW75 was P1, which indicates the original initiation position. The fatigue cracks propagated along with the deck thickness. The analysis results agreed well with the fatigue test results of DS80.

The leading ESS positions in DW75-W4 and DW75-W6 were marked as P2. The predicted initiation position was in good agreement with the DD80 result. Figure 8 exhibits the ESS of the weld seams and weld throats. The ESS of the weld throat of the outer weld seam (W1-1 and W1-2) decreased sharply with the introduction of the inner weld seam, and the probability of failure at the weld throat position was reduced.

The weld quality of the inner joints was inspected using visual inspection methods rather than advanced inspection equipment. The disadvantage of switching the crack site from the outer to the inner seam is that weld defects may appear at the inner welded joints, and the fatigue resistance of these joints may be reduced. More advanced inspection equipment should be employed to determine the weld quality of inner joints.

The addition of an inner weld seam can decrease the ESS of the outer weld root R1. Moreover, the inner weld seam can effectively protect the weld throat and improve its stiffness. The failure position changed from the weld toe of the outer seam to that of the inner seam, and the fatigue properties of the double-sided weld joints were better than those of the single-sided joints.

3.3 | Effect of loading mode and weld penetration ratio

According to Eurocode3 and AASHTO, two loading cases, that is, loading case I and case II, were defined for validating the fatigue performance variations of the OBD.

FIGURE 9A shows the ESS components in the specimen SW80-W6 in two loading cases. In loading case I, the maximum ESS of SW80-W6 was located on the weld toe of the outer seam P1. In loading case II, the maximum ESS of SW80-W6 appeared on the weld toe P3 and was more significant than loading case I. The ESS of the weld throats W1-1 and W1-2 were smaller than that of the deck-rib connection.

The ESS of the single-sided weld joints differed significantly among the various loading cases. The failure position changed from the outer seam toe to the deck-rib seam. The weld toe of the U-rib was regarded as the initiation position with higher stress than that of the weld toe and root, which were far from the weld seam.

Figure 9B demonstrates the ESS of the DW100-W4 components in loading cases I and II. The maximum ESS of the deck and U-rib in loading case I was located at the

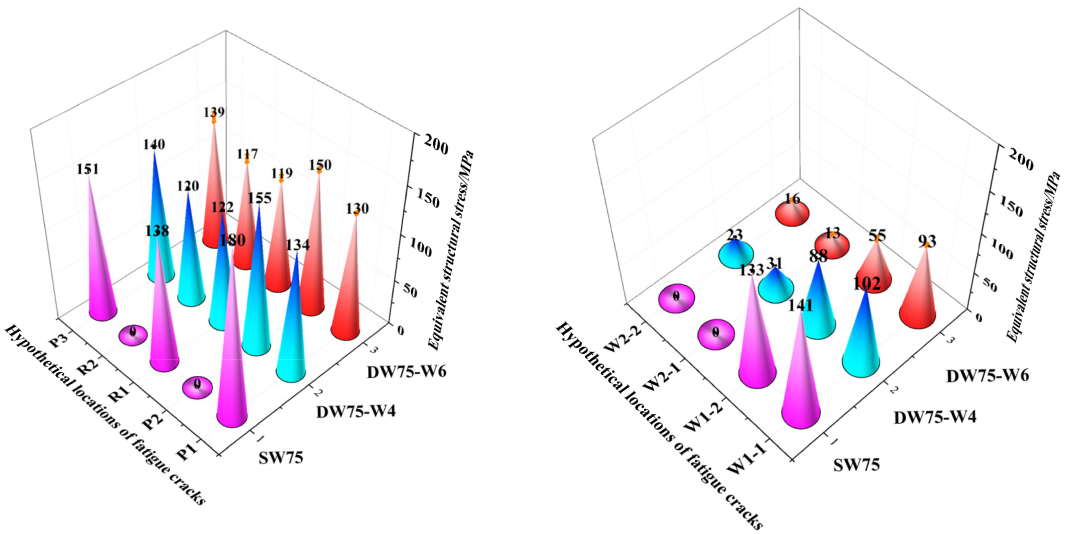

(A) Bridge deck and U-rib (B) Weld seam

FIGURE 8 (A,B) Equivalent structures stress (ESS) of various positions (load case I) [Colour figure can be viewed at wileyonlinelibrary.com]

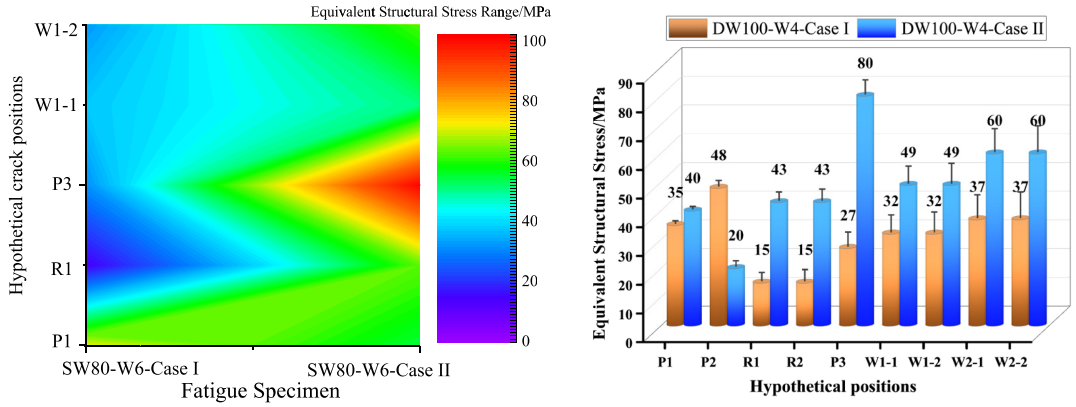

(A) Specimen SW80-W6

(B) Specimen DW100-W4

FIGURE 9 (A,B) Equivalent structures stress (ESS) of specimens in load cases I and II [Colour figure can be viewed at wileyonlinelibrary.com]

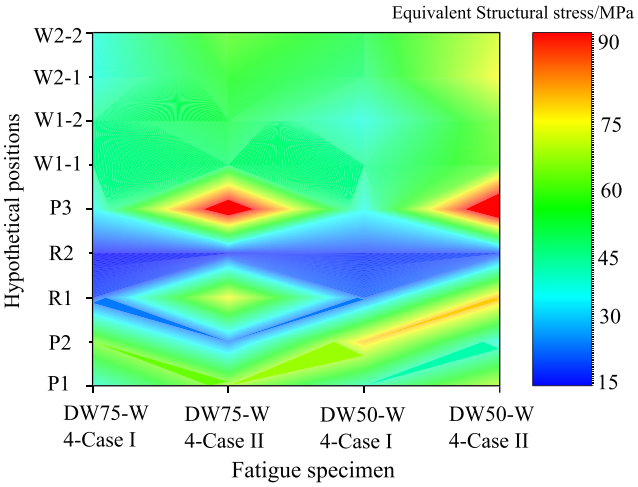

FIGURE 10 Equivalent structures stress (ESS) in load cases I and II [Colour figure can be viewed at wileyonlinelibrary.com]

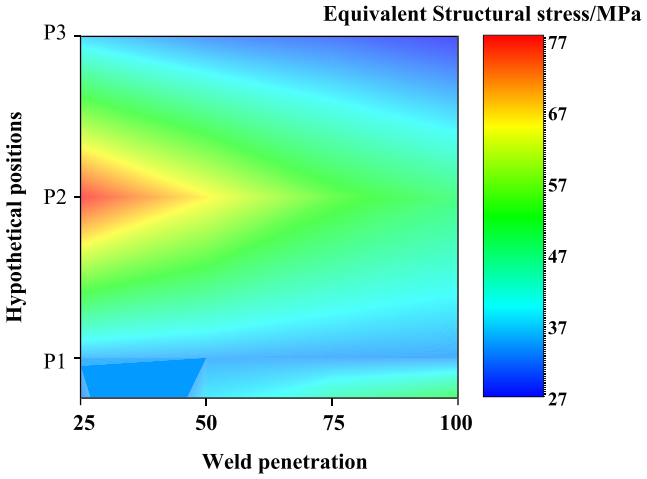

FIGURE 11 Equivalent structures stress (ESS) of fatigue cracks paths of P1, P2, and P3 in load case I [Colour figure can be viewed at wileyonlinelibrary.com]

inner seam toe. On the contrary, the maximum ESS in loading case II appeared at the weld toe of the deck-to-U-rib seam.

The crack initiation position in loading case I was at the inner weld toe, and the crack propagated along with the deck thickness. In contrast, in loading case II, the initiation was at the weld toe near the U-rib, and the fatigue cracks extended along with the U-rib thickness. The ESS of the DW75-W4 and DW50-W4 components are summarized in Figure 10. In loading case I, the maximum ESS of DW75-W4 and DW50-W4 was located at the inner weld seam toe. In loading case II, the maximum ESS of DW75-W4 and DW50-W4 appeared at the same position of the weld toe near the U-rib.

Analysis results indicate that the loading position changes the failure position from the weld toe of the outer seam to that near the U-rib. The fatigue properties of the welded joints in loading case I were better than those in loading case II. The loading mode significantly affects the fatigue properties of weld joints in OBD without considering the crossbeam.

The ESS of weld seams with various penetration ratios in loading case I was obtained. A more reasonable definition of the weld penetration ratio is given in Section 3.1, as shown in Figure 11. The weld penetration ratios were 25%, 50%, 75%, and 100%, considering the welding technology and differences in quality. The ESS of the weld toe of the outer weld seam P1 remained steady with the change in the weld properties. The ESS of the weld toe of the inner weld seam P2 reduced sharply by 60.4% with the increase of the weld penetration ratio. The ESS of the weld toe near the U-rib P3 decreased

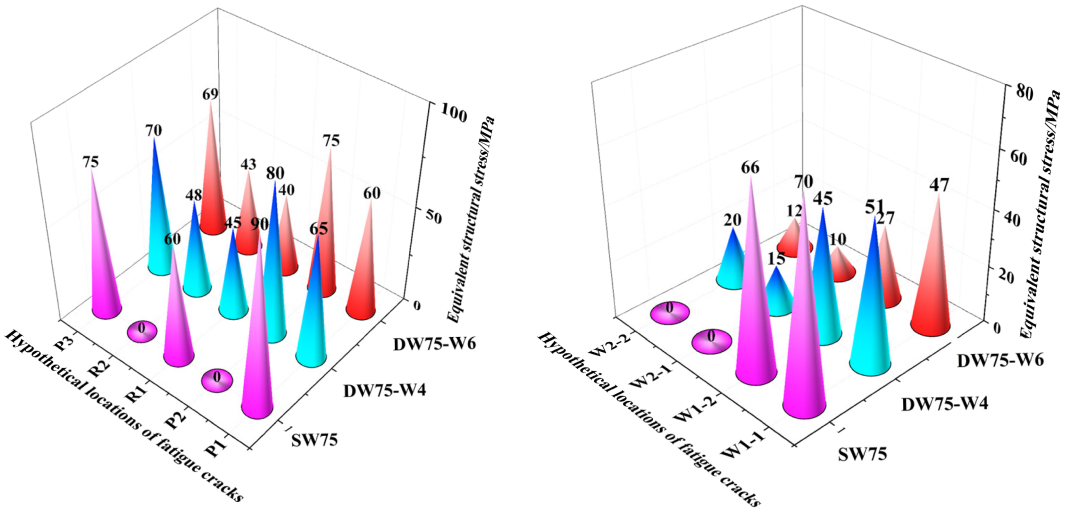

(A) the bridge deck and U-rib (B) weld seam

FIGURE 12 Equivalent structures stress (ESS) of the bridge deck and U-rib [Colour figure can be viewed at wileyonlinelibrary.com]

gradually by 37% when the weld penetration ratio was increased from 25% to 100%.

The ESS trend was consistent with fatigue test results reported by Maddox,[56] Kainuma,[57] Ya,[58] and Xing.[59] In addition, the results of P1 and P3 in the double-sided weld joints were consistent with those of single-sided joints reported by Wang.[31] The effect of the weld penetration ratio on the weld toe of the inner weld seam P2 and the outer weld throat W1 was more significant than that on the other positions.

3.4 | Effect of weld leg size

Previous studies have shown that the addition of an inner seam affects the fatigue properties of double-sided weld joints. Specimen models with various weld fillet sizes, that is, SW80-W6, DW80-W4, and DW80-W6, were investigated based on loading case I. The dimensions of the welded joints and potential initiation positions are presented in Figure 7D.

The ESS of the U-rib and weld seam with various weld fillet sizes was obtained, and the results are shown in Figure 12. The maximum ESS of SW80 was located at the weld toe of the outer seam. The maximum ESS of DW80-W4 appeared at the weld toe of the inner seam, while that of DW80-W6 was located at the weld toe of the inner seam. Compared to that in single-sided joints, the ESS of the weld root in double-sided weld joints was significantly reduced, indicating that double-sided weld joints can improve the load-bearing capacity and fatigue properties of weld roots. Furthermore, the ESS of the weld throats W1 and W2 in the double-sided weld joints was less significant than that in the single-sided joints.

The ESS of R1, R2, W1, and W2 in DW80-W6 was lower than DW80-W4. Comparative results indicate that the fatigue properties can be improved, and the weld throat can be protected by increasing the size of the inner weld fillet.

4 | CONCLUSIONS

In this paper, the effect of joint type, loading mode, weld penetration ratio, and weld fillet size on the fatigue failure mode of double-sided weld joints in OBD was investigated using the master *S-N* curve method.

1. It was validated that the master *S-N* curve method can capture various failure modes of double-sided weld joints in fatigue tests. All fatigue test result data of the three groups fell within the 99% confidence interval of the unified master *S-N* curve.
2. The failure position changed from the weld toe of the outer seam to that of the inner seam, and the fatigue properties of the double-sided weld joints were better than those of the single-sided joints. The inner weld seam can effectively protect the weld throat and improve its stiffness.
3. The effect of weld penetration ratio on the fatigue properties of the weld toe of the inner weld seam in the deck and outer weld throat was more significant than that at the other positions.
4. The fatigue properties can be improved, and the weld throat can be protected by increasing the size of the inner weld fillet.

The parameterized analysis presented in this paper has been derived on the basis of the master S-N curve method. It is rather concise and is readily available for extension into practical design guidance or specifications, which also involve effects of weld type, weld penetration, and weld leg size.

ACKNOWLEDGEMENTS

This research was funded by the National Key R & D Program of China (Grant No. 2019YFB1600702) and the Natural Science Foundation of China (Grant No. 51678191 and No. 51605116).

CONFLICT OF INTEREST

The authors declare no conflict of interest.

AUTHOR CONTRIBUTION

Haibo Yang: Conceptualization, methodology, data curation, writing–original draft, and writing–review & editing. **Ping Wang**: Funding acquisition, data curation, software, and writing–review & editing. **Hongliang Qian**: Supervision, funding acquisition, validation, and writing–review & editing. **Pingsha Dong**: Conceptualization and methodology.

DATA AVAILABILITY STATEMENT

The data that support the findings will be available in Haibo Yang at https://orcid.org/0000-0002-0632-3260 following an embargo from the date of publication to allow for commercialization of research findings.

NOMENCLATURE

ESS	equivalent structures stress
$F_{i,y}$	nodal forces along weld seams
$I(r)$	load mode effect factor
m	crack propagation parameter, $m = 3.6$
P/W/R	failure path definition symbol
r	bending stress ratio
S-N	stress versus fatigue cycle life
t	base metal thickness
t^*	referenced base metal thickness
y_i	nodal coordination
ΔS_s	equivalent structural stress range
$\Delta\sigma_s$	structural stress range
ρ	weld penetration
σ_b	bending traction structural stress
σ_m	membrane traction structural stress
σ_s	traction structural stress

ORCID

Haibo Yang https://orcid.org/0000-0002-0632-3260
Ping Wang https://orcid.org/0000-0003-1147-5477

REFERENCES

1. Shen S. Recent advances on the fundamental research of spatial structures in China. *Eng Struct*. 2006;2:93-103.
2. Zhu A, Li M, Zhu H, Xu GY, Xiao HZ, Ge HB. Fatigue behavior of orthotropic steel bridge decks with inner bulkheads. *J Constr Steel Res*. 2018;146:63-75.
3. Pfeil MS, Battista RC, Mergulhao AJR. Stress concentration in steel bridge orthotropic decks. *J Constr Steel Res*. 2005;61(8):1172-1184.
4. Ji B, Liu R, Chen C, Maeno H, Chen XF. Evaluation on root-deck fatigue of orthotropic steel bridge deck. *J Constr Steel Res*. 2013;90:174-183.
5. Shan C, Yi Y. Stress concentration analysis of an orthotropic sandwich bridge deck under wheel loading. *J Constr Steel Res*. 2016;122:488-494.
6. Maljaars J, Gration D, Vonk E, Dooren F. Crack growth prediction of deck plate-stiffener joints in orthotropic steel bridge decks. IABSE Symp Report. 2013;99:1571-1578.
7. Zhang Q, Bu Y, Li Q. Research progress on fatigue of orthotropic steel bridge deck. *China J Highway Trans*. 2017;30:14-30.
8. Meng F, Zhang QH, Xie HB, Zhang L, Li JP. *Key Technology of Anti-Fatigue of Orthotropic Steel Bridge Deck*. Beijing: People's Communications Press; 2014:1-30.
9. Yang HB, Wang P, Qian HL, Dong PS. Analysis of fatigue test conditions for reproducing weld toe cracking into U-rib wall in orthotropic bridge decks. *Int J Fatigue*. 2022;162:106976.
10. Van Puymbroeck E, Van Staen G, Iqbal N, Backer HD. Residual weld stresses in stiffener-to-deck plate weld of an orthotropic steel deck. *J Constr Steel Res*. 2019;159:534-547.
11. Shan C, Yi YH. An experimental and numerical study on the behavior of a continuous orthotropic bridge deck with sandwich construction. *Thin-Walled Struct*. 2017;111:138-144.
12. Wu W, Kolstein H, Veljkovic M. Fatigue resistance of rib-to-deck welded joint in OSDs, analyzed by fracture mechanics. *J Constr Steel Res*. 2019;162:105700.
13. Shigenobu K, Yang M, Jeong YS, Inokuchi S, Kawabata A, Uchida D. Experiment on fatigue behavior of rib-to-deck weld root in orthotropic steel decks. *J Constr Steel Res*. 2016;119:113-122.
14. Wang Y, Wang Z, Zheng Y. Analysis of fatigue crack propagation of an orthotropic bridge deck based on the extended finite element method. *Adv Civil Eng*. 2019;1:1-14.
15. Huang Y, Zhang Q, Bao Y, Bu YZ. Fatigue assessment of longitudinal rib-to-crossbeam welded joints in orthotropic steel bridge decks. *J Constr Steel Res*. 2019;159:53-66.
16. Wei Z, Jin H, Chen GL. Traction structural stress analysis of fatigue behaviors of girth butt weld within welded cast steel joints. *Int J Press Ves Pip*. 2020;179:1-22.
17. Sleczka L. Low cycle fatigue strength assessment of butt and fillet weld connections. *J Constr Steel Res*. 2004;60(3-5):701-712.
18. Fang Z, Ding YL, Wei XC, Li AQ, Geng FF. Fatigue Failure and Optimization of Double-sided Weld in Orthotropic Steel Bridge Decks. *Eng Fail Anal*. 2020;116:1-14.
19. Karakas O, Morgenstern C, Sonsino CM. Fatigue design of welded joints from the wrought magnesium alloy AZ31 by the local stress concept with the fictitious notch radii of r_f=1.0 and 0.05mm. *Int J Fatigue*. 2008;30(12):2210-2219.
20. Karakas O. Consideration of mean-stress effects on fatigue life of welded magnesium joints by the application of the Smith–

Watson–Topper and reference radius concepts. *Int J Fatigue*. 2013;49:1-17.
21. Karakas O, Zhang G, Sonsino CM. Critical distance approach for the fatigue strength assessment of magnesium welded joints in contrast to Neuber's effective stress method. *Int J Fatigue*. 2018;112:21-35.
22. Karakas O. Application of Neubers effective stress method for the evaluation of the fatigue behaviour of magnesium welds. *Int J Fatigue*. 2017;101:115-126.
23. Tao ZQ, Zhang M, Zhu Y, Cai T, Zhang ZL, Liu H. Multiaxial notch fatigue life prediction based on the dominated loading control mode under variable amplitude loading. *Fatigue Fract Eng Mater Struct*. 2021;44(1):225-239.
24. Luca S. Notches, nominal stresses, fatigue strength reduction factors and constant/variable amplitude multiaxial fatigue loading. *Int J Fatigue*. 2022;162:106941.
25. Ran Y, Liu JH, Xie LJ. Multiaxial fatigue life prediction method considering notch effect and non-proportional hardening. *Eng Fail Anal*. 2022;136:106202.
26. Aygul M, Al-Emrani M, Urushadze S. Modelling and fatigue life assessment of orthotropic bridge deck details using FEM. *Int J Fatigue*. 2012;40:129-142.
27. Chen Y, Lv P, Li DT. Research on fatigue strength for weld structure details of deck with U-rib and diaphragm in orthotropic steel bridge deck. *Metals*. 2019;5(5):484-500.
28. Chen B, Chen Z, Xie X, Ye XW. Fatigue performance evaluation for an orthotropic steel bridge deck based on field hot-spot stress measurements. *J Test Eval*. 2020;48(2):20180565.
29. Shen W, Yan R, He F, Wang SM. Multiaxial fatigue analysis of complex welded joints in notch stress approach. *Eng Frac Mech*. 2018;204:344-360.
30. Pei X, Ravi SK, Dong P, Li X, Zhou X. A multiaxial vibration fatigue evaluation procedure for welded structures in frequency domain. *Mech Syst Signal Process*. 2022;167:108516.
31. Wang P, Pei X, Dong P, Song S. Traction structural stress analysis of fatigue behaviors of rib-to-deck joints in orthotropic bridge deck. *Int J Fatigue*. 2019;125:11-22.
32. Pei X, Dong P, Xing S. A structural strain parameter for a unified treatment of fatigue behaviors of welded components. *Int J Fatigue*. 2019;124:444-460.
33. Pei X, Dong P, Kim MH. A simplified structural strain method for low-cycle fatigue evaluation of girth-welded pipe components. *Int J Fatigue*. 2020;139:105732.
34. Pei X, Dong P. An analytically formulated structural strain method for fatigue evaluation of welded components incorporating nonlinear hardening effects. *Fatigue Fract Eng Mater Struct*. 2019;42(1):239-255.
35. Kyuba H, Dong P. Equilibrium-equivalent structural stress approach to fatigue analysis of a rectangular hollow section joint. *Int J Fatigue*. 2005;27(1):85-94.
36. Dong P, Hong JK, Osage DA, Dewees D, Prager M. The Master S-N curve method an implementation for fatigue evaluation of welded components in the Asme B&Pv Code, Section Viii, Division 2, and API 579–1/Asme Ffs-1. WRC BULLETIN, 2010.
37. Li J, Zhang Q, Yuan DY, Guo YW, Bu YZ. Fatigue resistance evaluation for structural system of orthotropic steel bridge deck based on equivalent structural stress. *China J High Trans*. 2018;31:134-143.
38. Kim MH, Kang SW. Testing and analysis of fatigue behavior in edge details: A comparative study using hot spot and structural stresses. *Kyobu Geka, the Japan J Thor Surg*. 2008;61:331-334.
39. Li J, Zhang Q, Bao Y, Zhu JZ, Chen L, Bu YZ. An equivalent structural stress-based fatigue evaluation framework for rib-to-deck welded joints in orthotropic steel deck. *Eng Struct*. 2019;196:109304.
40. Bemessung Und Konstruktion von Stahlbauten: DIN EN 1993; Eurocode 3. 1–7. Plattenförmige Bauteile Mit Querbelastung: Deutsche Fassung EN 1993–:2007+AC:2009. 2010. Deutsche Norm. DIN EN 1993.
41. Cheng B, Cao X, Ye XH, Cao YS. Fatigue tests of welded connections between longitudinal stringer and deck plate in railway bridge orthotropic steel decks. *Eng Struct*. 2017;153:32-42.
42. Cheng B, Ye XH, Cao XE, Mbako DD, Cao YS. Experimental study on fatigue failure of rib-to-deck welded connections in orthotropic steel bridge decks. *Int J Fatigue*. 2017;103:157-167.
43. Zhang Q, Guo YW, Li J, Yuan DY, Bu YZ. Fatigue crack propagation characteristics of double-sided welded joints between steel bridge decks and longitudinal ribs. *China J High Trans*. 2019;32:49-56.
44. Liu Y, Chen F, Lu N, Wang L, Wang BW. Fatigue performance of rib-to-deck double-side welded joints in orthotropic steel decks. *Eng Fail Anal*. 2019;105:127-142.
45. Yang H, Wang P, Qian H. Fatigue behavior of typical details of orthotropic steel bridges in multiaxial stress states using traction structural stress. *Int J Fatigue*. 2020;141:105862.
46. Yang H, Wang P, Qian H. Fatigue property analysis of U rib-to-crossbeam connections under heavy traffic vehicle load considering in-plane shear stress. *Steel Compos Struct*. 2021;38:271-280.
47. Yang HB, Wang P, Qian HL, Niu S, Dong PS. An experimental investigation into fatigue behaviors of single- and double-sided U rib welds in orthotropic bridge decks. *Int J Fatigue*. 2022;159:106827.
48. You R, Liu P, Zhang D, Feng J, Zhu A. Experiments of fatigue performance of U-rib-to-deck connection with inner sides welding in orthotropic steel bridge deck. *J China Foreign High*. 2018;38:174-179.
49. Dong P. A structural stress definition and numerical implementation for fatigue analysis of welded joints. *Int J Fatigue*. 2001;23(10):865-876.
50. Dong P. A robust structural stress method for fatigue analysis of offshore/marine structures. *J Offshore Mech Arct Eng*. 2005;127(1):68-74.
51. Dong P, Prager M, Osage D. The design master S-N curve in ASME div 2 rewrite and its validations. *Weld World*. 2007;51(5-6):53-63.
52. Tamai S, Yagata Y, Hosoya T. New technologies in fabrication of steel bridges in Japan. *J Constr Steel Res*. 2002;58(1):151-192.
53. Yang HB, Wang P, Qian HL, Niu S, Dong PS. A Study of Fatigue Crack Propagation Paths at U-Rib Welds in Orthotropic Bridge Decks using a Phased-Array Imaging Technique. *Theor Appl Fract Mech*. 2022;119:103310.
54. Wang CS, Fu BN, Zhang Q, Feng Y. Fatigue test on full-scale orthotropic steel bridge deck. *China J High Trans*. 2013;26:69-76.

55. Wei ZZ, Pei XJ, Qian XD, Xing SZ, Feng LY, Jin H. Traction stress-based fatigue failure mode identification of load-carrying welded cruciform joints. *Int J Fatigue*. 2022;161:106897.
56. Maddox SJ. The fatigue behavior of trapezoidal stiffener to deck plate welds in orthotropic bridge decks. 1974.
57. Kainuma S, Yang M, Jeong YS, Inokuchi S, Kawabata A, Uchida D. Experimental investigation for structural parameter effects on fatigue behavior of rib-to-deck welded joints in orthotropic steel decks. *Eng Failure Ana*. 2017;79:520-537.
58. Ya S, Yamada K, Ishikawa T. Fatigue evaluation of rib-to-deck welded joints of orthotropic steel bridge deck. *J Bri Eng*. 2011; 16(4):492-499.
59. Xing S, Dong P. *A fatigue failure mode transition criterion for sizing load-carrying fillet-welded connections*. Vol. 1598. ASTM Special Tech Pub; 2017:258-277.

How to cite this article: Yang H, Wang P, Qian H, Dong P. Modeling of fatigue failure mode in U-rib to deck joints in orthotropic bridge structures. *Fatigue Fract Eng Mater Struct*. 2022; 45(9):2721-2733. doi:10.1111/ffe.13776